RSC Advances

PAPER

View Article Online
View Journal | View Issue

Cite this: *RSC Adv.*, 2026, **16**, 29218

The effect of Cr–Cu modification on the microbiologically influenced corrosion resistance of X70 pipeline steel

Junxiang Yang,[a] Xiaohu Zhang,[a] Yuzhou Chen,[a] Xiaolong Li,[a] Chao Liu,[a] Daiwei Guo,[b] Junlei Wang,[c] Jike Yang[d] and Zhong Li*[a]

Received 11th March 2026
Accepted 13th May 2026

DOI: 10.1039/d6ra02083f

rsc.li/rsc-advances

Microbiologically influenced corrosion (MIC) caused by sulfate-reducing bacteria (SRB) is a critical threat to the integrity and service life of oil and gas pipelines. This study developed a Cr–Cu-modified X70 pipeline steel by microalloying and evaluated its resistance to SRB-induced MIC. The MIC behavior of the modified steel and conventional X70 steel was examined in *Desulfovibrio vulgaris* cultures by biofilm quantification, weight-loss measurements, surface characterization, and electrochemical tests. Scanning electron microscopy (SEM), confocal laser scanning microscopy (CLSM), and electrochemical impedance spectroscopy (EIS) were used to assess biofilm formation, corrosion-product morphology, and interfacial electrochemical behavior. Biofilm quantification and cell counting showed reduced SRB attachment on Cr–Cu steel. Weight-loss measurements gave a corrosion rate of 0.186 mm per year, corresponding to an 8.8% decrease relative to X70 steel. SEM and CLSM revealed that Cr–Cu steel formed a denser corrosion-product layer. Cr enrichment promoted a compact Cr_2O_3-containing passive film, which limited extracellular electron transfer and suppressed localized corrosion. EIS further confirmed higher charge-transfer resistance and improved film stability during immersion. The enhanced MIC resistance is attributed to the combined effects of Cr-induced passivation and weakened sulfide-assisted corrosion due to the reduced Cu content.

1. Introduction

Microbiologically influenced corrosion (MIC) is a major corrosion issue involving the accelerated degradation of metals and alloys by microbial metabolism and associated by-products.[1–3] In the oil and gas industry, MIC represents a major threat to the structural integrity of long-distance pipeline networks, resulting in massive economic losses and environmental hazards globally.[4,5] Among the diverse microbial communities found in these environments, sulfate-reducing bacteria (SRB) are widely recognized as the most prevalent and destructive anaerobic microorganisms responsible for MIC.[6–8] The core mechanisms of MIC involve electrochemical interactions among microbial metabolites, corrosion products, and the biofilm–substrate interface.

To mitigate MIC in engineering applications, conventional environmental control strategies primarily rely on organic surface coatings, cathodic protection (CP), and the routine injection of chemical biocides. However, these external interventions exhibit significant limitations in complex service environments. For instance, SRB can colonize and accumulate within the crevices of disbonded coatings, where the geometric shielding effect prevents CP currents from effectively reaching the metal substrate, thereby intensifying localized pitting.[9–12] Moreover, the continuous and long-term application of biocides inevitably induces antimicrobial resistance within the biofilms and raises severe ecological toxicity concerns. Compared with these environmental and chemical control strategies, intrinsic material design has received considerably less attention, yet it provides a more durable, reliable, and "built-in" defense against microbial attacks.[13,14]

API 5L X70 pipeline steel is extensively utilized in modern long-distance, high-pressure transportation systems owing to its excellent combination of high strength, good weldability, and cost-effectiveness.[15] Nevertheless, under moist and anaerobic conditions—such as buried soils, subsea environments, or oilfield produced water—conventional X70 steel is highly prone to SRB-MIC.[16] Although previous studies have investigated the environmental factors, CP interference, and general electrochemical behaviors of pipeline steels under SRB environments, research dedicated to mitigating MIC through intrinsic material design and metallurgical tailoring remains largely insufficient.[17]

Cr additions generally promote the formation of compact and stable Cr-enriched passive films, which improve surface barrier properties and reduce interfacial reactivity. Furthermore, Cu

[a]*Key Laboratory for Corrosion and Protection (MOE), National Materials Corrosion and Protection Data Center, Institute for Advanced Materials and Technology, University of Science and Technology Beijing, Beijing 100083, China. E-mail: zhongli@ustb.edu.cn*

[b]*IDQ Science and Technology Development (Hengqin, Guangdong) Co. Ltd., Guangdong, China*

[c]*Defense Engineering Institute, AMS, PLA, Luoyang, 471000, China*

[d]*School of Materials and Engineering, University of Science and Technology Beijing, Beijing 100083, China*

readily reacts with hydrogen sulfide (H_2S) produced by SRB, potentially accelerating localized SRB-MIC attack, including pitting.[18] Therefore, coordinated adjustment of Cr and Cu contents may provide a pathway toward improved SRB-MIC resistance, a topic that has received limited attention to date.

Despite these complexities, previous studies on Cu- and Cr-containing steels have mainly focused on utilizing their individual antibacterial or corrosion-resistant effects. However, less attention has been paid to low-alloy compositional regulation within the conventional X70 pipeline steel framework.[19] In particular, the combined effect of moderate Cr enrichment and reduced Cu level on SRB-MIC behavior remains insufficiently understood. The mechanistic significance of such coordinated compositional tuning, especially in relation to passivation stability, sulfide-related interfacial reactions, and localized corrosion development under SRB exposure, therefore remains an important knowledge gap.

To address this gap, a Cr–Cu modified X70 pipeline steel, hereafter referred to as Cr–Cu steel, was designed in this work through targeted microalloying based on conventional X70 steel. Within this low-alloy design, the Cr level was moderately increased to improve initial passivation, whereas the Cu level was maintained at a lower level to reduce Cu-sulfide-related interfacial reactivity under SRB exposure. This compositional strategy differs from conventional high-Cr alloyed steels, as it employs moderate Cr microalloying within the standard X70 pipeline steel matrix, thereby offering improved cost-effectiveness and industrial applicability in MIC-prone environments. More importantly, this study integrates elevated Cr content with reduced Cu level to specifically combat SRB-induced MIC, representing a synergistic compositional strategy that has rarely been explored in traditional Cr-bearing steel designs. Unlike most existing Cr-alloyed steels that mainly focus on general corrosion resistance, the present work addresses MIC by simultaneously suppressing EET-MIC and M-MIC mechanisms under SRB exposure. Using commercial X70 steel as a reference, the effects of this compositional modification on SRB colonization, corrosion-product evolution, and localized MIC behavior were systematically investigated. The significance of this work lies not merely in improving MIC resistance, but in demonstrating that coordinated Cr enrichment and lower Cu level can jointly influence passive-film stability, SRB attachment, and localized corrosion evolution, thereby providing a mechanism-guided alloy design concept for MIC-resistant pipeline steels.

2. Materials and methods

2.1. Culture media and materials

Cr–Cu steel and X70 steel were machined into square (10 mm × 10 mm) specimens. The chemical compositions (wt%) of the two types of materials are listed in Table 1. All specimens were ground sequentially with SiC papers of 400, 800, and 1000 grits, then rinsed with absolute ethanol, dried, and sterilized.

The SRB strain used in this study was *D. vulgaris*, which was incubated in ATCC 1249 medium (pH 7.0 ± 0.2) at 37 °C. The composition of ATCC 1249 is listed in Table 2. To remove dissolved oxygen, the medium was purged with high-purity nitrogen gas for 1 h after preparation. The dissolved oxygen concentration, measured using a dissolved oxygen meter, was 0 mg L^{-1} before inoculation. All anaerobic procedures were carried out in an anaerobic chamber under a nitrogen atmosphere. Within the chamber, each anaerobic bottle was filled with 200 mL of ATCC 1249 medium and inoculated with 2 mL of *D. vulgaris* seed. $Fe(NH_4)_2(SO_4)_2$ was added to the medium to eliminate residual oxygen prior to inoculation. For each material type, both a sterile control and an SRB-MIC group were established.

2.2. Cell counts

After seven days of anaerobic incubation, three parallel specimens were retrieved from each bottle, rinsed with phosphate-buffered saline (PBS, pH 7.4), and gently swabbed to detach the surface biofilm and adherent cells. The collected material was suspended in PBS, transferred to a conical tube, and vortexed for 30 s to obtain a homogeneous suspension. In parallel, 1 mL of culture medium from each group was diluted with 9 mL of PBS and vortexed for 30 s to prepare planktonic cell suspensions. Both suspensions were enumerated using a hemocytometer under 400× optical microscopy (OMAX 40X-2000X, OMAX, USA). The pH of the culture media associated with the two steel types was measured to assess microbial activity and environmental changes relevant to SRB-MIC behavior. For each condition, multiple parallel specimens were used within the same anaerobic bottle to assess the reproducibility of the measurements.

2.3. Weight loss

According to the ASTM G1-03 standard,[20] all specimens were ground, cleaned, dried, and labeled before testing. The original weight of each specimen was measured using an electronic balance (Shimadzu AUW220D, Shimadzu, Japan). After a seven-days immersion period, the specimens were cleaned by a rust removal solution composed of 500 mL H_2O, 500 mL HCl, and 3.5 g hexamethylenetetramine. The two specimen types were sequentially rinsed with deionized water and absolute ethanol, dried under ambient conditions, and then reweighed to determine mass loss. The SRB-MIC corrosion rate (CR, mm per year) for each material type was determined from six parallel specimens from the same anaerobic culture bottle. The corrosion rate was calculated using eqn (1):

$$CR = \frac{8.76 \times 10^4 \times \Delta m}{\rho A t} \quad (1)$$

Table 1 Chemical compositions (wt%) of the X70 and Cr–Cu steels

	C	Mn	Cr	Mo	Ni	Nb	V	Si	Al	Ti	Cu	S	P	Fe
Cr–Cu	0.049	1.077	0.231	0.129	0.193	0.050	0.036	0.280	0.023	0.016	0.008	0.005	<0.001	Bal.
X70	0.064	1.242	0.026	0.145	0.177	0.038	0.025	0.210	0.037	0.011	0.140	0.005	0.007	Bal.

Table 2 Chemical composition of ATCC 1249 medium

Component	Chemical	Amount
Component I	$MgSO_4 \cdot 7H_2O$	4.1 g
	Sodium citrate	5.0 g
	$CaSO_4 \cdot 2H_2O$	1.0 g
	NH_4Cl	1.0 g
	Distilled water	400 mL
Component II	K_2HPO_4	0.5 g
	Distilled water	200 mL
Component III	Yeast extract	1.0 g
	Sodium lactate	4.5 mL
	Distilled water	200 mL
Component IV	$Fe(NH_4)_2(SO_4)_2$	1 g
	Distilled water	200 mL

where Δm is the average weight loss (g), ρ is the density of the steel (7.85 g cm^{-3} for X70 steel), A is the surface area (cm^2), and t is the immersion time (h).

2.4. Biofilm and rust layer analysis

The biofilm morphology was characterized by SEM (GeminiSEM 500, Carl Zeiss, Oberkochen, Germany). After a 7 days incubation period, all specimens were first gently rinsed with PBS to remove loosely attached cells and SRB-MIC products. To characterize the biofilms, the specimens were fixed with 2.5% (w/w) glutaraldehyde at 10 °C for 8 h, followed by dehydration in a graded ethanol series (50%, 70%, 80%, 90%, 95%, and 100% v/v). A gold coating was applied to facilitate electrical conductivity.[21]

The coupon cross-sections were sequentially ground with 400-, 800-, and 1000- grit sandpaper to characterize the morphology of the SRB-MIC product layer. After cleaning and drying, the morphology of the SRB-MIC product layer was examined by SEM and EDS.

2.5. MIC pit morphology characterization

Following biofilm observations, the SRB-MIC corrosion product layer was chemically removed to expose the underlying substrate. The morphology of SRB-MIC pits was subsequently characterized using SEM and CLSM (Zeiss LSM780, Carl Zeiss, Oberkochen, Germany).

2.6. MIC product analysis

The composition of SRB-MIC corrosion products formed on the specimen surfaces was analyzed by X-ray diffraction (XRD, D8 Advance, Bruker, Karlsruhe, Germany), which provided detailed information on their phase composition and structural characteristics.[22]

2.7. Electrochemical analysis

Electrochemical measurements were conducted using an electrochemical workstation (Model VersaSTAT 4A, Princeton Applied Research, Oak Ridge, TN, USA). Cr–Cu steel and X70 steel specimens served as the working electrodes, with a saturated calomel electrode (SCE) as the reference electrode and a platinum sheet as the counter electrode (a three-electrode system). All tests were performed under anaerobic conditions.[23] The electrochemical tests included open circuit potential (OCP), electrochemical impedance spectroscopy (EIS), and linear polarization resistance (R_p). On the 7th day, cathodic and anodic potentiodynamic polarization curves were obtained at a scan rate of 0.167 mV s^{-1} over a potential range of −200 mV to +200 mV *versus* OCP.

3. Results and discussion

3.1. Cell counts and weight loss

Fig. 1 shows the sessile and planktonic cell counts for Cr–Cu steel and X70 steel after seven days of immersion in *D. vulgaris* broth. The results indicate that the sessile cell count of Cr–Cu steel was approximately $8.90 \times 10^6 \pm 8.21 \times 10^5$ cells per cm^2, while the planktonic cell count reached $6.10 \times 10^6 \pm 1.32 \times 10^5$ cells per mL. In contrast, X70 steel exhibited a higher sessile cell count of $1.07 \times 10^7 \pm 4.54 \times 10^5$ cells per cm^2 and $7.10 \times 10^6 \pm 4.02 \times 10^5$ cells per mL planktonic cells. The lower sessile cell count in Cr–Cu steel suggests that although the reduced copper content weakens its direct bactericidal effect against SRB, Cu–Cr alloy modification can still suppress SRB growth and proliferation.

Fig. 2 shows the weight loss and corrosion rates of Cr–Cu steel and X70 pipeline steel in the SRB and sterile environments. The average SRB-MIC rate of X70 pipeline steel was $0.204 \pm 1.68 \times 10^{-2}$ mm per year, whereas that of Cr–Cu steel was $0.186 \pm 3.02 \times 10^{-2}$ mm per year, which was lower than that of X70 steel. In sterile culture medium for seven days, the corrosion rates of Cr–Cu steel and X70 steel were $4.55 \times 10^{-2} \pm 9.97 \times 10^{-3}$ mm per year and $4.54 \times 10^{-2} \pm 8.35 \times 10^{-3}$ mm per year, which were significantly lower than in the SRB environment. A recent study reported corrosion rates of approximately 0.18 mm per year for Cr–Cu steel and 0.39 mm per year for X70 steel under similar SRB-exposure conditions, further confirming the observed trend.[24]

In SRB environments, Cu-related SRB-MIC proceeds primarily *via* a metabolite-induced mechanism (M-MIC). This process is dominated by the spontaneous chemical reaction between biogenic sulfide species (mainly HS^-) and metallic Cu, as described by the following thermodynamically favorable reaction:[25]

$$2Cu + HS^- + H^+ \rightarrow Cu_2S + H_2(g) \quad (2)$$

$$Cu + HS^- + H^+ \rightarrow CuS + H_2(g) \quad (3)$$

The negative Gibbs free energy change ($\Delta G' = -58.3$ kJ mol^{-1} for Cu_2S) indicates a strong thermodynamic driving force for copper sulfide formation. Alloys with higher Cu content provide more active Cu sites, facilitating sulfide adsorption and promoting the formation of copper sulfide MIC products, thereby accelerating MIC.[25]

Reducing the Cu content effectively limits the availability of reactive Cu sites and weakens the interaction between Cu and sulfide metabolites produced by SRB. This suppresses

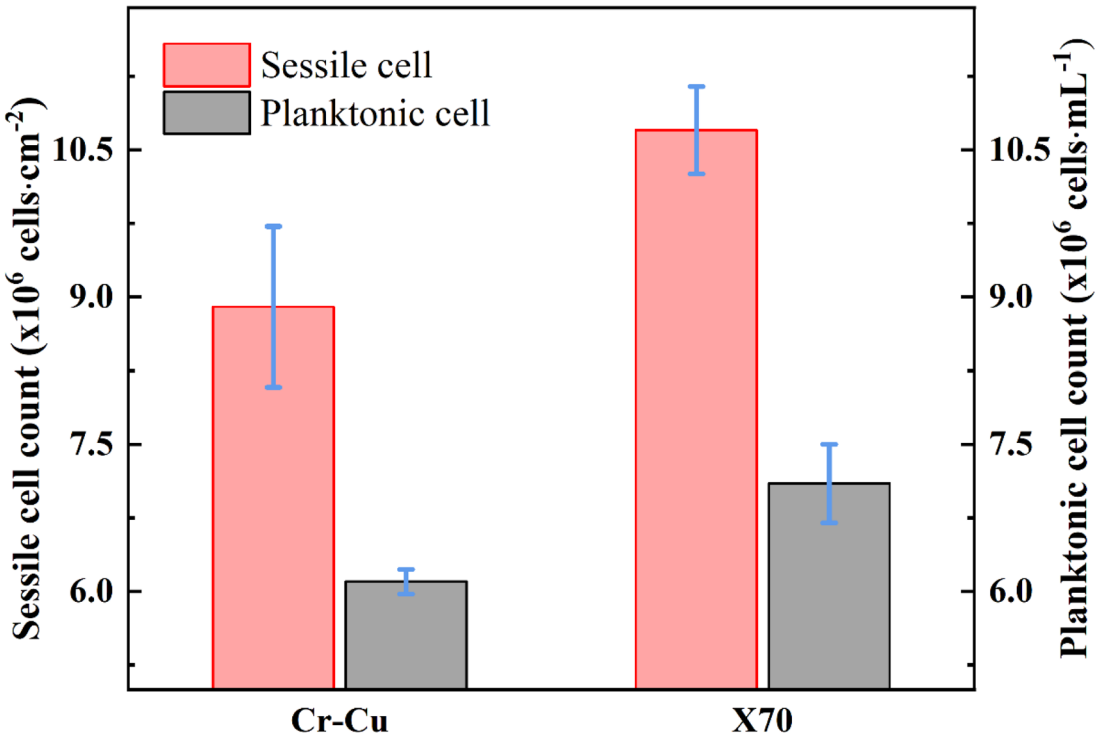

Fig. 1 Sessile and planktonic cell counts in the broth of Cr–Cu steel and X70 steel after seven days of immersion. (Each scatter band is the standard deviation of 5 independent samples).

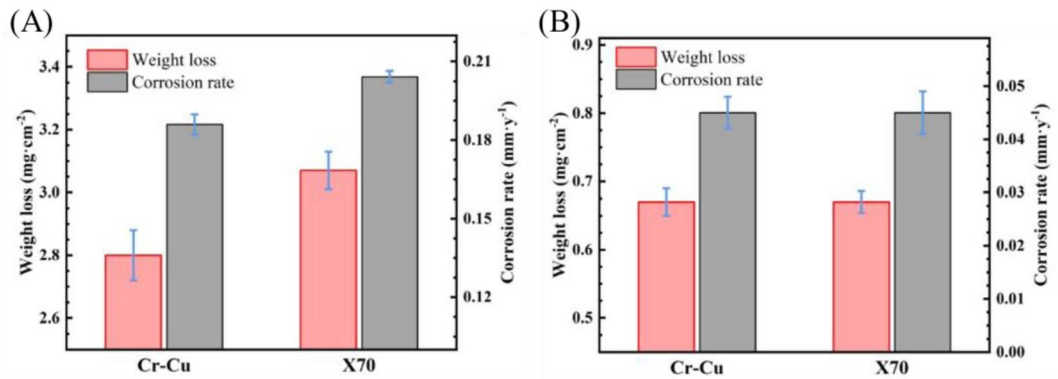

Fig. 2 Weight loss and MIC rates of Cr–Cu steel and X70 steel in the SRB (A) and sterile (B) environments. (Each scatter band represents the standard deviation of 6 independent samples, with the highest and lowest values excluded).

nucleation and growth of Cu_2S and reduces interfacial reactions between the metal surface and bacterial metabolites, thereby markedly decreasing the overall corrosion rate.

Furthermore, the SRB-MIC rate results are consistent with the cell counts, indicating that EET-related processes contributed to MIC. EET-MIC primarily involves the direct reduction of Fe by SRB, which can be inferred from localized iron dissolution, Fe^{2+} accumulation, and the associated MIC morphology observed in this study. The increased Cr content in Cr–Cu steel contributed to the formation of a thin Cr_2O_3-containing native passive film on the steel surface prior to immersion, as Cr reacted with oxygen in air during specimen preparation and exposure before the experiment:[26]

$$2Cr + \frac{3}{2}O_2 \rightarrow Cr_2O_3 \quad (4)$$

Dissolved oxygen measurements showed that the test solution was oxygen-free during immersion. Therefore, the Cr_2O_3 detected in this work is considered to originated mainly from the native oxide and passive film formed on the steel surface upon exposure to air before immersion. This pre-existing Cr-containing passive film acts as a physical and electrochemical barrier, reducing interfacial reactivity and thereby mitigating microbiologically influenced corrosion.[27]

3.2. Surface, biofilm, and MIC product analyses

Fig. 3 shows the surface morphologies of Cr–Cu steel and X70 steel after seven days of immersion in sterile and SRB environments. In the sterile environment, both Cr–Cu steel (Fig. 3A) and X70 steel (Fig. 3B) exhibited smooth surfaces, showing only minor surface irregularities and slight corrosion features. In contrast, pronounced differences were observed after exposure to the *D. vulgaris* broth. As shown in Fig. 3C, the Cr–Cu steel exhibited relatively limited SRB-MIC, with fewer MIC pits. In contrast, heavily localized SRB-MIC pits were observed on the surface of X70 steel (Fig. 3D). This difference in pit morphology and severity is consistent with the SRB-MIC rate results, indicating that the Cr–Cu steel shows better resistance to SRB-MIC. As indicated by eqn (2)–(4), Cr–Cu modification not only reduces the copper content, thereby mitigating M-MIC, but also mitigates the EET-MIC pathway through the formation of a Cr_2O_3 passive film. These two effects act synergistically, resulting in a comparatively smoother surface morphology.[28]

Fig. 4 shows the biofilm morphologies formed on Cr–Cu steel and X70 steel after seven days of immersion in the SRB environment. As illustrated in Fig. 4A, the biofilm formed on Cr–Cu steel exhibits a relatively uniform, network-like architecture with small and homogeneously distributed pores. Such morphology indicates that the diffusion and aggregation of SRB microcolonies during the adhesion stage can be mitigated. The ordered, porous structure facilitates balanced transport of nutrients and metabolites, thereby reducing local electrochemical heterogeneities and the tendency toward SRB-MIC pitting corrosion. This observation is consistent with the lower sessile cell counts observed for Cr–Cu steel.

In contrast, the biofilm on X70 steel (Fig. 4B) appears irregular, with SRB colonies randomly aggregated and forming locally thick extracellular polymeric substance (EPS) layers.[29] The heterogeneity of SRB-MIC pits distribution and uneven spatial agreement creates localized microenvironments with fluctuating pH and sulfide concentrations, which could enhance localized electrochemical activity and accelerate SRB-MIC.[30]

Fig. 5 presents the cross-sectional SEM images and corresponding elemental maps of the corrosion products, together with the residual biofilm, formed on Cr–Cu steel and X70 pipeline steel after 7 days of immersion in the SRB-containing medium. A clear difference in rust-layer morphology can be observed between the two steels. For Cr–Cu steel, the corrosion product layer is comparatively thin, compact, and laterally uniform, with a relatively smooth steel/rust interface and only limited evidence of severe local penetration. The associated elemental distributions are also more confined to a narrow interfacial region, indicating the development of a more compact corrosion-product/biofilm assemblage. By contrast, X70 steel exhibits a markedly thicker and more heterogeneous surface layer, characterized by a rougher outer morphology and a highly undulated steel/rust interface, implying enhanced localized attack beneath the deposits. The broader distribution of corrosion products and sulfur-containing species further suggests a less protective and less stable interfacial layer under SRB exposure. In addition, the residual biofilm on Cr–Cu steel

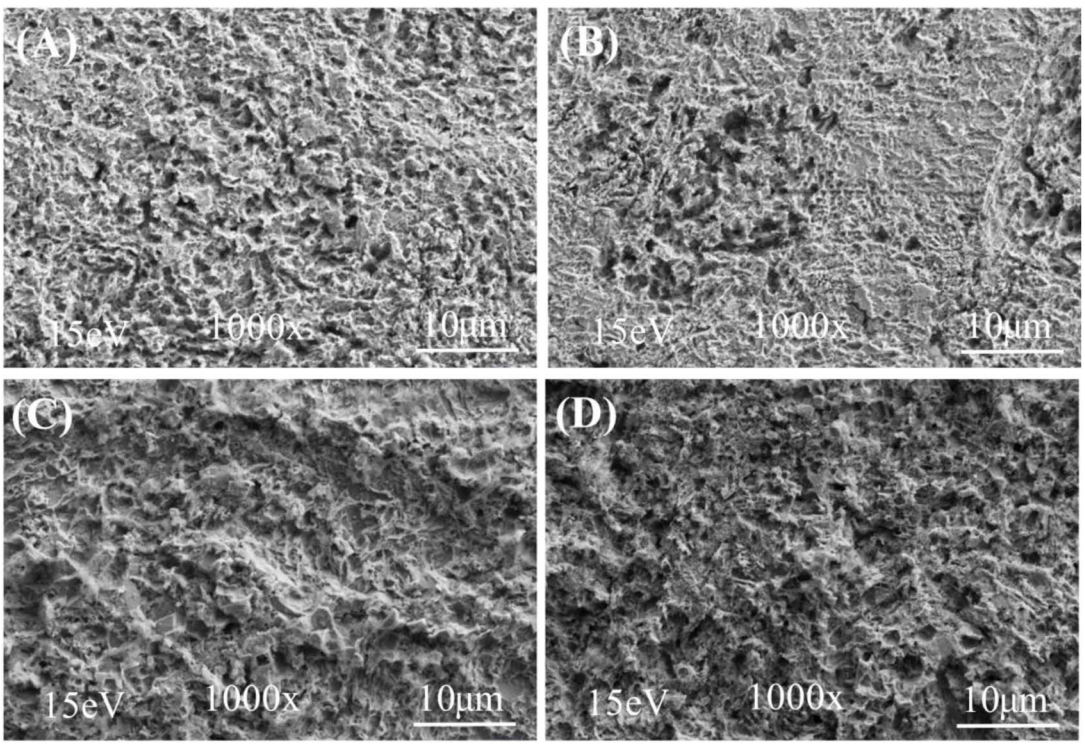

Fig. 3 Surface morphologies of Cr–Cu steel immersed in sterile (A), X70 steel immersed in sterile (B), Cr–Cu steel immersed in *D. vulgaris* (C), and X70 steel immersed in *D. vulgaris* (D).

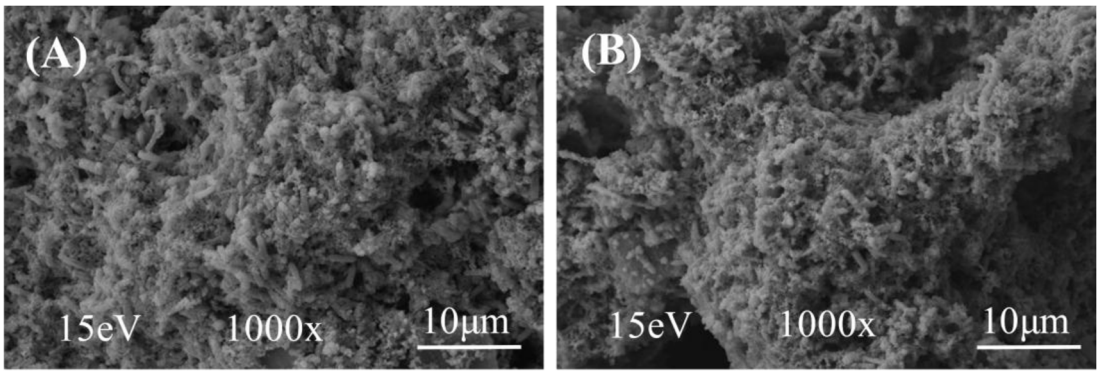

Fig. 4 Biofilm morphologies of Cr–Cu steel (A) and X70 steel (B) after seven days of immersion.

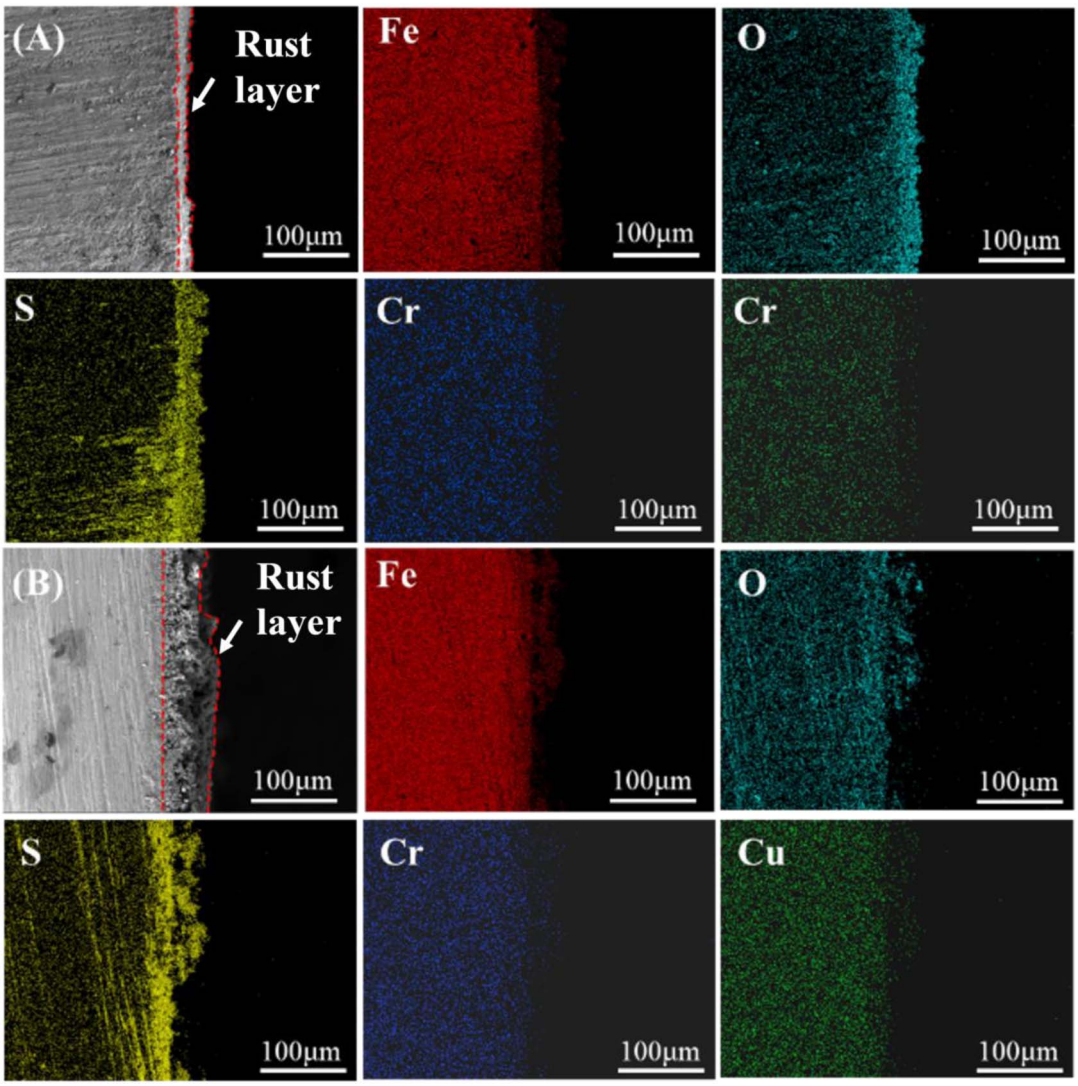

Fig. 5 SEM images of rust layers on Cr–Cu steel (A) and X70 pipeline steel (B) after seven days of immersion in the SRB environment.

appears less abundant than that on X70 steel, supporting the view that Cr–Cu alloying suppresses biofilm accumulation and thereby mitigates microbially influenced localized corrosion. Overall, the cross-sectional evidence indicates that Cr–Cu steel favors the formation of a denser and more protective interfacial layer, whereas X70 steel is more susceptible to uneven rust growth and localized deterioration in the SRB environment.

Fig. 6 presents the CLSM images and statistical distributions of SRB-MIC pitting depth for Cr–Cu steel and X70 steel after seven days of immersion in sterile and SRB environments. The average represents the average pit depth, and σ denotes the standard deviation of pit depth.[31] A larger σ indicates a more non-uniform distribution of pit sizes. Under sterile conditions, both steels that exhibited relatively smooth surfaces with shallow and uniformly distributed pits, reflected by lower average pitting depths (7.26 μm for Cr–Cu steel and 7.60 μm for X70 steel) and smaller standard deviations ($\sigma \approx 1.10$ μm), indicating minimal and uniform corrosion. In contrast, immersion in the SRB environment resulted in significantly deeper and more heterogeneous SRB-MIC pitting corrosion. Specifically, Cr–Cu steel (Fig. 6C) showed a moderate increase in average pitting depth to 11.32 μm with a standard deviation of 2.35 μm, while X70 steel (Fig. 6D) exhibited the most severe localized SRB-MIC attack, with the highest average pitting depth to 16.07 μm and a standard deviation of 3.20 μm. The increased σ values reflect greater dispersion in pitting depth, indicating more aggressive, localized corrosion behavior in the presence of SRB. Furthermore, the Cr–Cu steel exhibited a smoother corrosion morphology with fewer, shallower SRB-MIC pits, indicating superior SRB-MIC resistance. Biofilm formation is inversely correlated with increasing Cr content and decreasing Cu, and corresponds with SRB-MIC pits, which is consistent with the EET-MIC mechanism.[32,33]

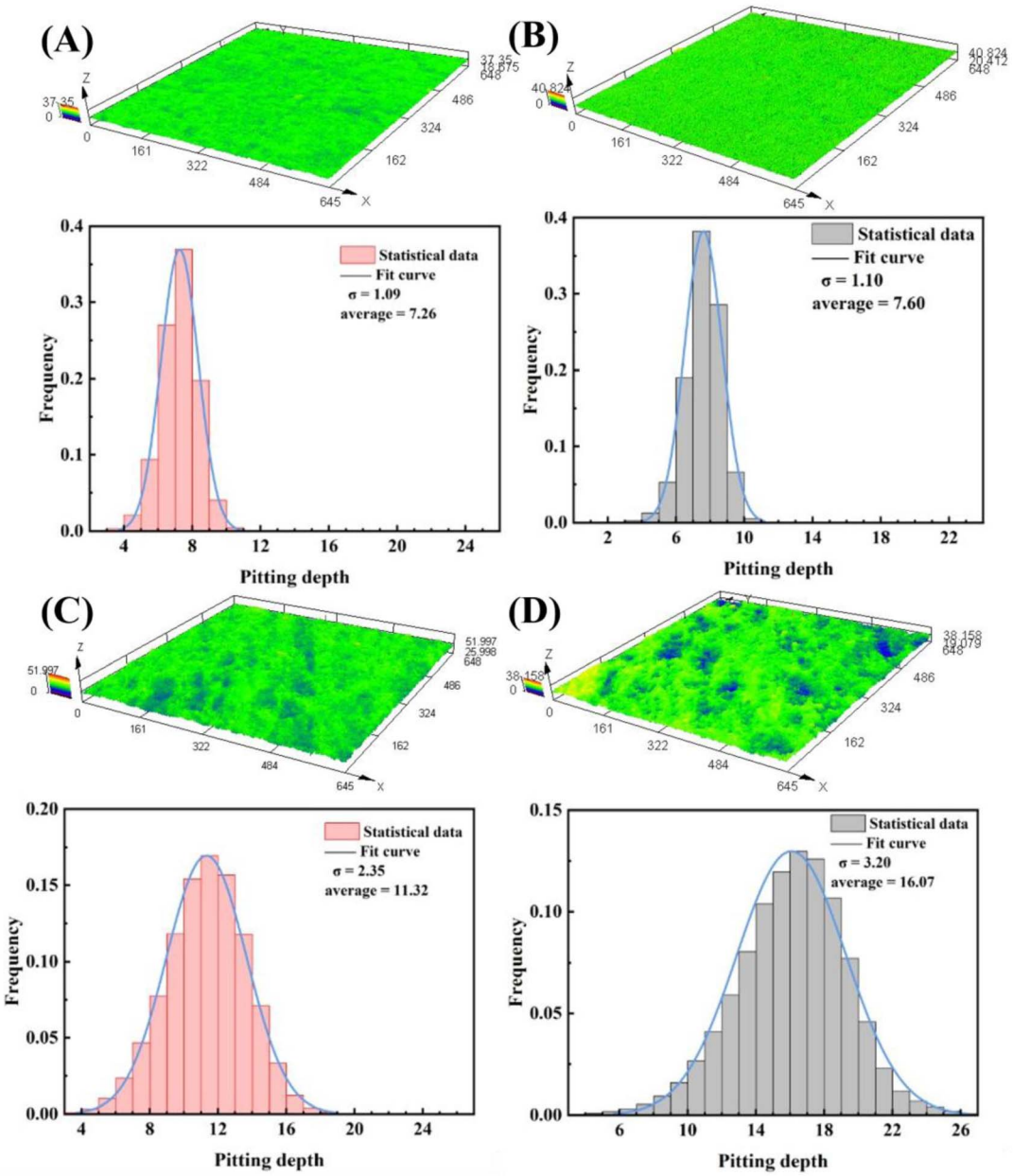

Fig. 6 CLSM images of corrosion pits (green) and statistical analysis of pitting depth (column) after immersion in sterile, Cr–Cu steel (A) and X70 steel (B); immersed in SRB, Cr–Cu steel (C) and X70 steel (D) after seven days.

These morphological observations are consistent with the surface analysis and SRB-MIC rate, indicating that a greater number of SRB-MIC pits corresponds to higher SRB sessile cell count and a faster SRB-MIC rate. The pitting characteristics further agree well with the biofilm morphology, weight-loss results, and sessile cell counts. This relationship suggests that EET-MIC is positively correlated with pit formation. Under sterile conditions, only a few shallow pits are observed. Taken together, the SEM and CLSM results indicate that corrosion under SRB exposure was dominated by localized attack rather than uniform dissolution. The Cr_2O_3 passive film effectively suppresses EET-MIC, while the reduced Cu content further inhibits M-MIC. The synergistic effects of these two factors decrease both the number and depth of SRB-MIC pits on Cr–Cu steel.

Fig. 7 presents the pH evolution of the culture media for Cr–Cu steel and X70 steel after seven days of immersion. The optimal growth pH for *D. vulgaris* is approximately 7.50,[34] while the initial pH of the medium was 7.00 ± 0.1. After seven days of incubation, the pH increased to 7.38 ± 0.04 for X70 steel and 7.14 ± 0.08 for Cr–Cu steel. In both cases, the broth became slightly alkaline (>7.0), indicating that hydrogen-ion corrosion played a negligible role in the overall SRB-MIC process. The gradual increase in pH can be attributed to the metabolic activity of SRB, during which sulfate is reduced to sulfide, as described by the following reactions.[25]

$$SO_4^{2-} + 4H_2 + H^+ \rightarrow HS^- + 4H_2O \quad (5)$$

$$Fe^{2+} + HS^- \rightarrow FeS + H^+ \quad (6)$$

$$H^+ + HS^- \rightarrow H_2S(g) \quad (7)$$

The generated HS^- is converted to H_2S, which escapes from the solution into the anaerobic bottle headspace, losing H in the broth and increasing the broth pH.[11,35] A similar alkalinization effect has been reported when SRB are used to neutralize acidic mine drainage.[34]

Fig. 8 presents the XRD patterns of the corrosion products formed on Cr–Cu steel and X70 steel after 7 days of exposure to the SRB-containing environment. For both steels, FeS is identified as the dominant crystalline phase, indicating that sulfide precipitation governs corrosion-product formation under the present SRB-MIC conditions. This observation is consistent with eqn (5)–(7), which describe the reaction between dissolved Fe^{2+} and biogenic sulfide species. In addition to the FeS peaks, several weak reflections can be tentatively assigned to Cr_2O_3 and Cu_2O, suggesting the presence of minor alloy-related oxide phases in the surface layers. However, their markedly lower intensities compared with those of FeS indicate that these oxides are secondary constituents rather than the primary corrosion products. Overall, the corrosion products formed on both steels are dominated by FeS, suggesting that the two steels follow a similar sulfide-controlled corrosion-product evolution pathway, while the main difference lies in the contribution of minor alloy-related oxides.

3.3. Electrochemical tests

3.3.1 OCP and R_p analysis. Fig. 9 illustrates the evolution of OCP and R_p for Cr–Cu steel and X70 steel during seven days of immersion in the SRB-MIC environment. The OCP of Cr–Cu steel remained consistently more positive than that of X70 steel, indicating a lower thermodynamic tendency toward SRB-MIC.

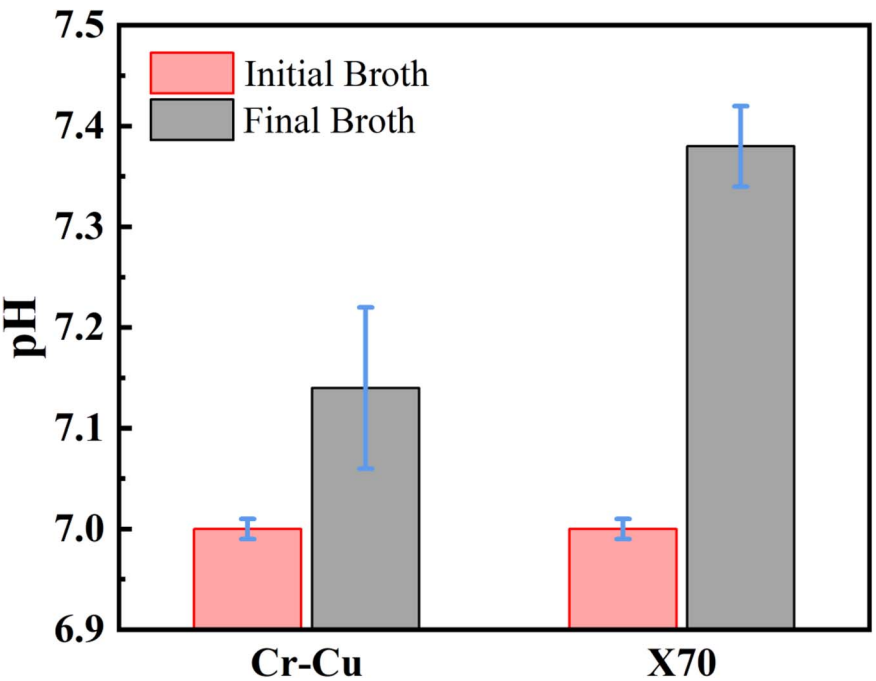

Fig. 7 Broth pH of Cr–Cu steel and X70 steel after seven days of immersion. (Each scatter band is the standard deviation of 3 independent samples).

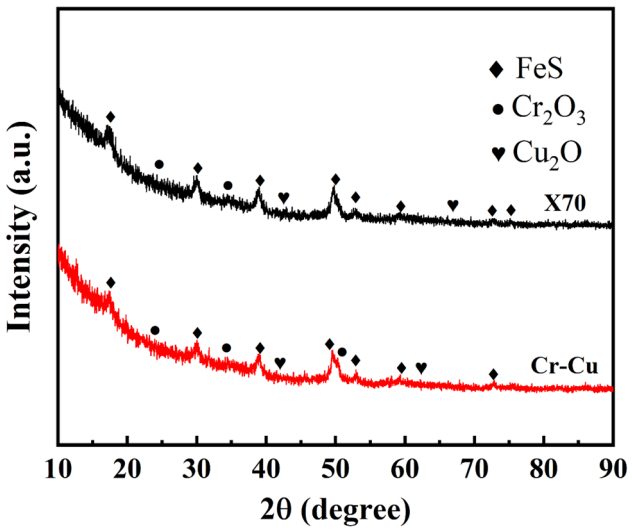

Fig. 8 XRD patterns of corrosion products on Cr–Cu steel and X70 steel after seven days of immersion.

In general, a more noble mixed potential, consistent with a more stable surface/interface. Therefore, the elevated OCP values of Cr–Cu steel suggest that Cr–Cu modification enhances surface stability and mitigates SRB-MIC susceptibility under SRB conditions.

As shown in Fig. 9B, the R_p values decreased with increasing immersion time. During the first 3 days, Cr–Cu steel exhibited markedly higher R_p values than X70 steel, indicating superior resistance to SRB-MIC at the early stage of exposure. This electrochemical behavior is consistent with the weight-loss measurements, sessile cell counts, SEM observations, and pit statistical analysis, all of which demonstrate the enhanced corrosion resistance of Cr–Cu steel compared with X70 steel. However, after 3 days, the R_p values of both steels stabilized and exhibited no significant difference. This apparent convergence does not necessarily indicate identical corrosion behavior; rather, it is attributed to the progressive formation of biofilm/corrosion-product layers on both steel surfaces, which caused the corrosion process to evolve from an early charge-transfer-dominated stage to a film/diffusion-influenced stage. Under such conditions, R_p, as an overall polarization–resistance parameter, became less sensitive to the intrinsic interfacial differences between the two steels, leading to similar R_p values. To gain deeper insight into the evolution of the SRB-MIC processes and to clarify the underlying electrochemical mechanisms responsible for this behavior, EIS measurements were further conducted.[36]

3.3.2 EIS tests. EIS measurements for Cr–Cu steel and X70 steel in the SRB-containing medium are shown in Fig. 10, and the fitted parameters are listed in Table 3. The Nyquist plots show that Cr–Cu steel consistently exhibits a larger capacitive arc than X70 steel, while the Bode plots reveal a higher low-frequency impedance modulus throughout immersion, indicating a higher interfacial impedance and better resistance to SRB-induced corrosion. These results suggest that Cr–Cu modification suppresses interfacial electrochemical activity and improves the stability of the surface film/corrosion-product layer.

At day 1, the spectra of both steels are well fitted by the R(QR)(QR) circuit (Fig. 11), indicating contributions from both the surface film and charge-transfer process. In this stage, Cr–Cu steel shows higher R_f and R_{ct} values than X70 steel, suggesting the formation of a more protective initial surface film and lower early-stage SRB-MIC susceptibility. On days 3 and 7, the spectra are better described by the R(Q(RW)) circuit, indicating a transition to a film/diffusion-controlled process. The appearance of the Warburg element reflects increasing mass-transport limitation through the biofilm/corrosion-product layer.[37] Meanwhile, Q_f decreased from the 10^{-2} to 10^{-4} order of magnitude and n_1 increases from 0.52 to 0.71, indicating thickening and progressive homogenization of the surface layer.

Although both steels exhibit diffusion-influenced behavior at longer immersion times, Cr–Cu steel retains a slightly higher R_f at day 7, whereas X70 steel shows larger Warburg-

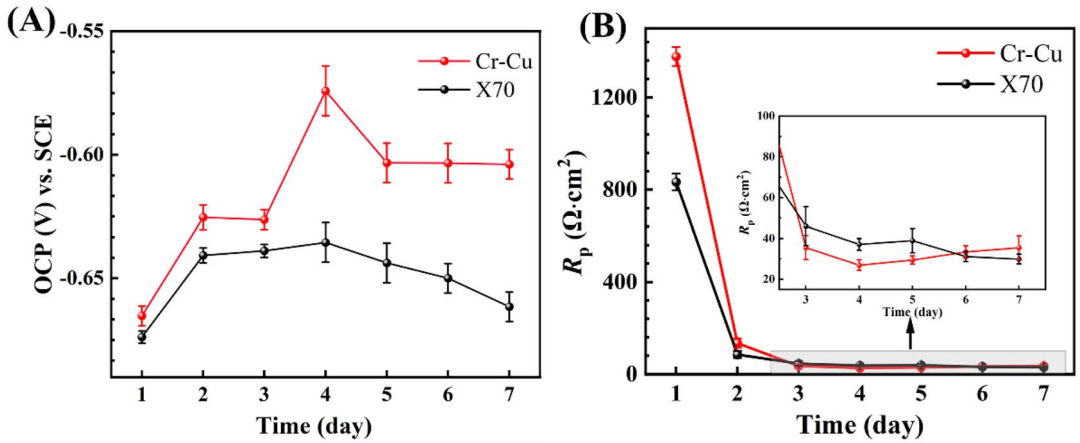

Fig. 9 Variation of OCP (A) and R_p (B) for Cr–Cu steel and X70 steel during seven days of immersion. (Each scatter band is the standard deviation of 5 independent samples).

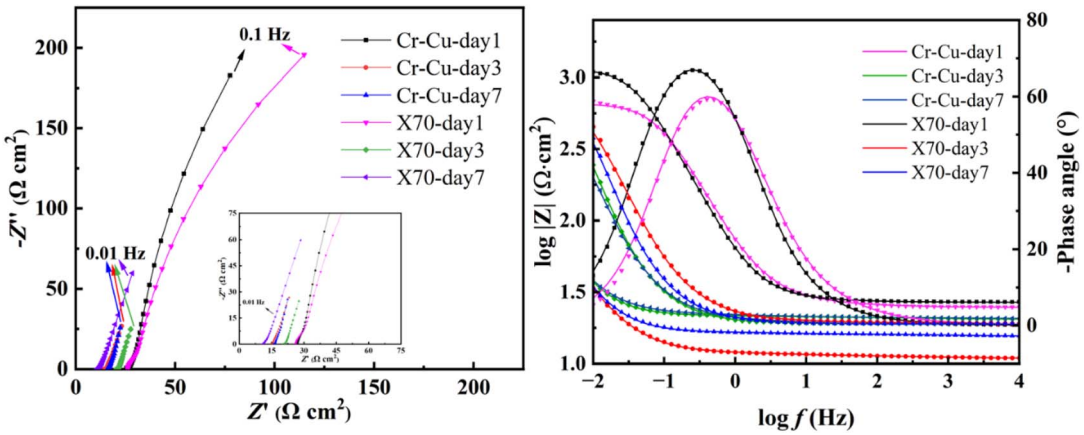

Fig. 10 Nyquist plots and Bode plots of Cr–Cu steel and X70 steel during 7 days of immersion.

Table 3 Equivalent circuit fitting parameters corresponding to Fig. 10

	Day	R_s (Ω cm^2)	R_f (Ω cm^2)	Q_f (Ω^{-1} s^{-n} cm^{-2})	n_1	R_{ct} (Ω cm^2)	Q_{dl} (Ω^{-1} s^{-n} cm^{-2})	n_2	W_1–R (Ω cm^2)	W_1–T (s)	W_1–P	$\chi 2 \times 10^{-3}$
Cr–Cu	1	26.84	31.12	4.02×10^{-2}	0.52	1094	3.52×10^{-3}	0.97	—	—	—	0.24
	3	10.91	0.38	4.80×10^{-4}	0.72	—	—	—	1.63	0.41	0.39	0.53
	7	15.58	0.44	2.61×10^{-4}	0.76	—	—	—	1.50	0.52	0.42	0.83
X70	1	24.71	19.64	2.21×10^{-2}	0.52	614.2	3.03×10^{-3}	0.95	—	—	—	1.32
	3	20.49	0.60	4.91×10^{-4}	0.71	—	—	—	1.57	0.58	0.42	0.22
	7	20.66	0.34	2.57×10^{-4}	0.77	—	—	—	3.26	1.24	0.40	0.58

related parameters, indicating a stronger diffusion-controlled contribution associated with a thicker and less protective surface layer.[38] In addition, the W–P value of Cr–Cu steel is closer to 0.5, suggesting more homogeneous diffusion behavior.[39] Overall, Cr–Cu steel exhibits higher initial charge-transfer resistance and a more stable surface layer during prolonged SRB exposure, resulting in better resistance to SRB-MIC than X70 steel.

The fitting quality was evaluated by χ^2, and the low χ^2 values (0.22×10^{-3} to 1.32×10^{-3}) indicate satisfactory agreement between the experimental spectra and the fitted equivalent circuit models.

Although no direct mathematical correlation was established between pit depth and electrochemical parameters, the observed trends were consistent: more severe localized corrosion corresponded to less favorable electrochemical behavior.

3.3.3 Tafel curves analysis. Fig. 12 presents the potentiodynamic polarization curves of Cr–Cu steel and X70 steel after seven days of immersion in the *D. vulgaris* broth, with the corresponding data summarized in Table 4. The corrosion potential (E_{corr}) values of both steels suggest that thermodynamic tendencies toward SRB-MIC were similar. The SRB-MIC current density (i_{corr}) of Cr–Cu steel (100.9 μA cm^{-2}) was significantly lower than that of X70 steel (115.5 μA cm^{-2}), indicating a reduced SRB-MIC rate. This Tafel result is consistent with the weight-loss measurements, sessile cell counts, SEM observations, pit statistical analysis, R_p evolution, and EIS parameters. These results demonstrate that the Cr–Cu modification enhances SRB-MIC resistance of X70 steel.

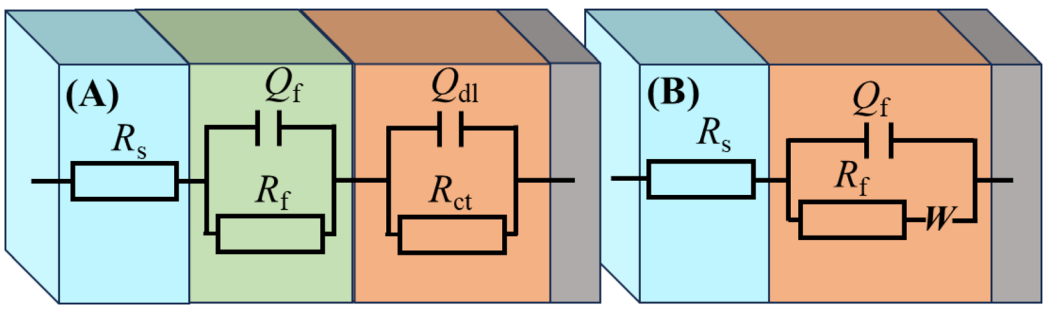

Fig. 11 Equivalent circuit models corresponding to Fig. 10: (A) two-time-constant model without diffusion elements used for both steels on day 1; (B) two-time-constant model with diffusion elements used for both steels on days 3 and 7.

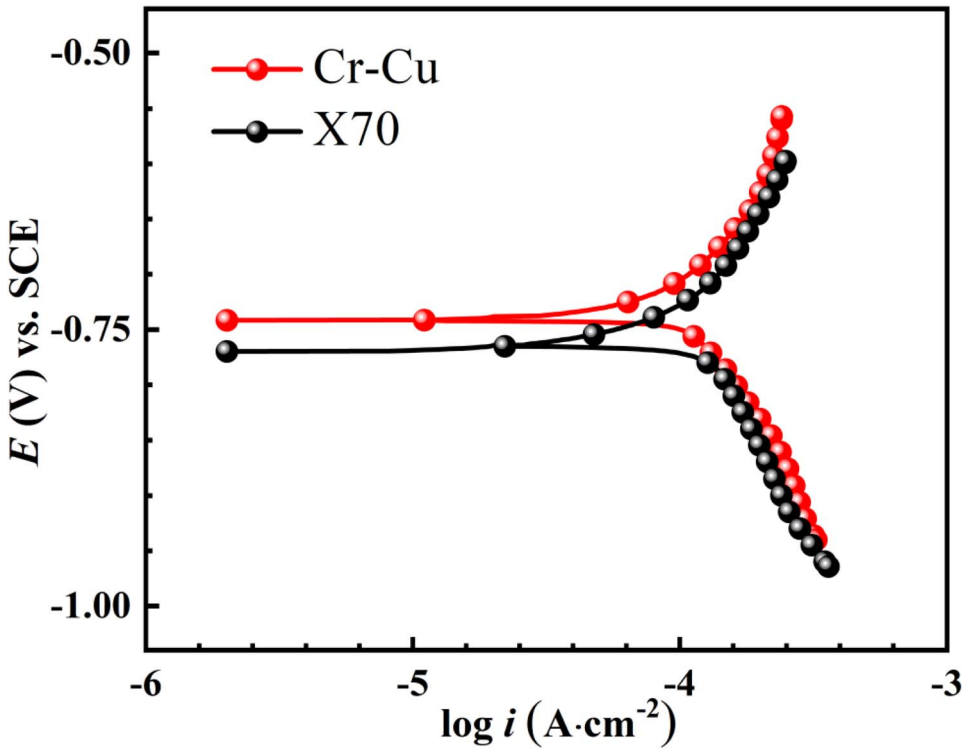

Fig. 12 Potentiodynamic polarization curves of Cr–Cu steel and X70 steel after seven days of immersion.

Table 4 Fitting parameters of the potentiodynamic polarization curves shown in Fig. 12

	i_{corr} ($\mu A\ cm^{-2}$)	E_{corr} (V) vs. SCE	b_a ($mV\ dec^{-1}$)	b_c ($mV\ dec^{-1}$)
Cr–Cu steel	1.01×10^2	−0.72	3.27×10^2	-3.60×10^2
X70 steel	1.16×10^2	−0.73	3.80×10^2	-5.14×10^2

4. Conclusion

The effect of coordinated Cr–Cu modification on the SRB-MIC behavior of X70 pipeline steel was systematically evaluated in *D. vulgaris* medium. During the 7 days anaerobic exposure, the modified steel exhibited improved resistance to MIC compared with conventional X70 steel, as evidenced by an 8.8% reduction in corrosion rate, reduced sessile-cell attachment, less severe localized attack, and shallower average pits.

Cross-sectional and surface characterizations further showed that Cr–Cu steel developed a thinner, denser and more uniform corrosion-product/biofilm layer, whereas X70 steel was associated with a thicker and more heterogeneous interfacial layer and more pronounced localized deterioration. Electrochemical measurements were consistent with these observations, with Cr–Cu steel showing a more noble OCP, a lower corrosion current density, and a higher initial interfacial resistance, indicating improved film stability and suppressed interfacial electrochemical activity under SRB exposure.

The improved MIC resistance is attributed to the synergistic effect of moderate Cr enrichment and reduced Cu content. Cr enrichment favors the formation of a compact Cr-containing passive film that limits interfacial electron transfer and mitigates localized dissolution, whereas lowering the Cu level decreases sulfide-assisted interfacial reactivity and thereby weakens metabolite-related corrosion. These results demonstrate that modest compositional regulation within the conventional X70 alloy framework can effectively improve resistance to SRB-induced MIC, and provide a mechanistically guided alloy-design strategy for pipeline steels operating in anaerobic microbial environments.

Future work should evaluate the Cr–Cu modified steel under longer exposure durations, in mixed microbial communities representative of real industrial environments, and under more field-relevant service conditions. Further studies will also aim to deepen the mechanistic understanding of the coordinated roles of Cr and Cu in MIC resistance and to assess the engineering applicability of this low-alloy compositional strategy.

Author contributions

Y. J. X.: writing – review & editing; visualization; supervision; project administration; methodology; conceptualization. Z. X. H.: writing – review & editing. C. Y. Z: writing – review & editing; project administration. L. X. L.: writing – review & editing; visualization; data curation. L. C.: methodology; investigation; formal analysis; conceptualization. G. D. W.: writing – review & editing. W. J. L.: writing – review & editing, project

administration. Y. J. K.: writing – review & editing. L. Z.: writing – review & editing, project administration, funding acquisition.

Conflicts of interest

All authors declare no financial or non-financial competing interests.

Data availability

The data supporting the findings of this study are included within the article. All experimental data generated or analyzed during this study are provided in the figures and tables of this manuscript.

Acknowledgements

This work was supported by the National Natural Science Foundation of China (grant numbers 52401074), the Fundamental Research Funds for the Central Universities (FRF-BD-25-039), the National Materials Corrosion and Protection Data Center, and the Key Laboratory for Corrosion and Protection (MOE).

References

1 W. P. Iverson, Microbial corrosion of metals, *Adv. Appl. Microbiol.*, 1987, **32**, 1–36.
2 Y. Lou, H. Zhang, Z. Li, S. Liu, W. Chang, H. Qian, X. Hao and D. Zhang, Light-driven extracellular electron transfer accelerates microbiologically influenced corrosion by Rhodopseudomonas palustris TIE-1, *Corros. Sci.*, 2024, **237**, 112309.
3 W. Chang, H. Qian, Z. Li, A. Mol and D. Zhang, Application and prospect of localized electrochemical techniques for microbiologically influenced corrosion: a review, *Corros. Sci.*, 2024, **236**, 112246.
4 K. Maji and M. Lavanya, Microbiologically influenced corrosion in stainless steel by *Pseudomonas aeruginosa*: an overview, *J. Bio- Tribo-Corros.Publisher: Springer*, 2024, **10**, 16.
5 B. Hou, X. Li, X. Ma, C. Du, D. Zhang, M. Zheng, W. Xu, D. Lu and F. Ma, The cost of corrosion in China, *npj Mater. Degrad.*, 2017, **1**, 4.
6 T. Gu, J. Ru, R. Jia, U. Tuba and D. Xu, Toward a better understanding of microbiologically influenced corrosion caused by sulfate reducing bacteria, *J. Mater. Sci. Technol.*, 2019, **35**(4), 631–636.
7 D. Xu, Y. Li and T. Gu, Mechanistic modeling of biocorrosion caused by biofilms of sulfate reducing bacteria and acid producing bacteria, *Bioelectrochemistry*, 2016, **110**, 52–58.
8 T. T. T. Tran, K. Kannoorpatti, A. Padovan and S. Thennadil, Sulphate-reducing bacteria's response to extreme pH environments and the effect of their activities on microbial corrosion, *Appl. Sci.*, 2021, **11**(5), 2201.
9 T. Liu and Y. F. Cheng, The influence of cathodic protection potential on the biofilm formation and corrosion behaviour of an X70 steel pipeline in sulfate reducing bacteria media, *J. Alloys Compd.*, 2017, **729**, 180–188.
10 J. Wang, H. Li, M. Du, M. Sun and L. Ma, Study on mechanism underlying the acceleration of pitting corrosion of B30 copper-nickel alloy by sulfate-reducing bacteria in seawater, *Sci. Total Environ.*, 2024, **928**, 172645.
11 Z. Li, J. Yang, S. Lu, W. Dou and T. Gu, Stress corrosion cracking failure of X80 carbon steel U-bend caused by *Desulfovibrio vulgaris* biocorrosion, *J. Mater. Sci. Technol.*, 2024, **174**, 95–105.
12 L. Benea, E. Danaila and P. Ponthiaux, Effect of titania anodic formation and hydroxyapatite electrodeposition on electrochemical behaviour of Ti-6Al-4V alloy under fretting conditions for biomedical applications, *Corros. Sci.*, 2015, **91**, 262–271.
13 X. Shi, W. Yan, D. Xu, M. Yan, C. Yang, Y. Shan and K. Yang, Microbial corrosion resistance of a novel Cu-bearing pipeline steel, *J. Mater. Sci. Technol.*, 2018, **34**(12), 2480–2491.
14 X. Zhang, C. Yang and K. Yang, Contact killing of Cu-bearing stainless steel based on charge transfer caused by the microdomain potential difference, *ACS Appl. Mater. Interfaces*, 2019, **12**(1), 361–372.
15 D. Sun, D. Wang, L. Li, K. Gong, S. Ren, F. Xie and M. Wu, Study on stress corrosion behavior and mechanism of X70 pipeline steel with the combined action of sulfate-reducing bacteria and constant load, *Corros. Sci.*, 2023, **213**, 110968.
16 L. Zhu, Y. Tang, J. Jiang, Y. Zhang, M. Wu, C. Tang, T. Wu and K. Zhao, Microbial corrosion behavior of pipeline steels in simulation environment of natural gas transportation pipeline, *RSC Adv.*, 2023, **13**(51), 36168–36180.
17 D. He, L. Li, W. Guo, G. He, P. Peng, T. Shao, H. Huan, G. Zhang, G. Han and J. Yan, Improvement in oxidation resistance of Ti2AlNb alloys at high temperatures by laser shock peening, *Corros. Sci.*, 2021, **184**, 109364.
18 Z. Xu, T. Gu, Y. Ding, R. He, Y. Fan, T. Zhang, H. Wan, Y. He, Y. Xiong and H. Liu, Microbial corrosion of high manganese austenitic steel by a sulfate reducing bacterium dominated by extracellular electron transfer and intergranular effect, *Corros. Sci.*, 2025, **248**, 112799.
19 Y. Wu, Z. Li, D. Wang, Z. Tian, B. Liu, Z. Zhou, T. Gu, F. Wang and D. Xu, Combination of Cr-Cu-bearing pipeline steel and novel biocides as a strategy to combat microbiologically influenced corrosion, *Corros. Sci.*, 2025, **248**, 112807.
20 ASTM International, *ASTM G1-03: Standard Practice for Preparing, Cleaning, and Evaluating Corrosion Test Specimens*, ASTM International, West Conshohocken, PA, 2003.
21 N. Li, L. Wang, Z. Zhou, X. Jiang, H. Yu and D. Sun, The interaction mechanism of titanium alloy TC4 between passive film and sulfate reducing bacteria biofilm in marine environment, *Appl. Surf. Sci.*, 2025, **690**, 162620.
22 J. Cheng, Y. Wu, J. Duan, G. Polat, S. Hong and J. Cheng, The influence of SRB on corrosion behavior of Cu-based medium-entropy alloy coating sprayed by HVOF, *Bioelectrochemistry*, 2024, **156**, 108633.

23 Y. Pu, W. Dou, Y. F. Cheng, S. Chen, Z. Xu and Z. Chen, Biogenic H_2S and extracellular electron transfer resulted in two-coexisting mechanisms in 90/10 Cu-Ni alloy corrosion by a sulfate-reducing bacteria, *Corros. Sci.*, 2023, **211**, 110911.

24 L. Fan, Y. Sun, D. Wang, Y. Zhang, M. Zhang, E. Zhou, D. Xu and F. Wang, Microbiologically influenced corrosion of a novel pipeline steel containing Cu and Cr elements in the presence of Desulfovibrio vulgaris Hildenborough, *Corros. Sci.*, 2023, **223**, 111421.

25 W. Dou, R. Jia, P. Jin, J. Liu, S. Chen and T. Gu, Investigation of the mechanism and characteristics of copper corrosion by sulfate reducing bacteria, *Corros. Sci.*, 2018, **144**, 237–248.

26 N. Chen, Y. Hu, X. Song, Q. Feng, S. Wang, B. Li, H. Zhang, Y. Tan, W. Liu, H. Wang and K. Xiao, Mitigating synergistic corrosion of X60 steel under SRB and AC interference: Optimal CP potentials, *Electrochim. Acta*, 2025, **539**, 147041.

27 S. Lu, L. Zhang, N. Xue, S. Chen, M. Xia, M. Fu, Y. Gao and W. Dou, Riboflavin-mediated Fe0-to-microbe electron transfer corrosion of EH40 steel by Halomonas titanicae, *Corros. Sci.*, 2024, **231**, 111981.

28 Z. Li, J. Yang, S. Lu and T. Gu, X80 U-bend stress corrosion cracking (SCC) crack tip dissolution by fast corroding *Desulfovibrio ferrophilus* IS5 biofilm, *Process Saf. Environ. Prot.*, 2023, **178**, 56–64.

29 Y. Hao, R. Xu, H. Bi, Z. Zhang, Z. Chen, M. Li and B. Chen, The corrosion properties of ferritic stainless steel with varying Cr and Mo contents in the early stages of a simulated proton exchange membrane fuel cell environment investigated using experimental and joint calculation method HKD, *Corros. Sci.*, 2024, **239**, 112389.

30 C. Zhu, Y. Pu, Z. Guo, Y. Hou, S. Hou, F. Feng, B. Zhang, C. Dong, D. Tang and S. Chen, Gravity-driven corrosion effects in microbiologically influenced corrosion: Circumferential corrosion distribution of 90/10 Cu-Ni alloy by *Desulfovibrio vulgaris*, *Corros. Sci.*, 2025, **254**, 113049.

31 L. Zhu, J. Wu, D. Zhang, P. Wang, C. Li, Y. Wang and Z. Sun, The difference in preferential corrosion of 2205 duplex stainless steel induced by *Pseudomonas aeruginosa* between full and alternate immersion, *Corros. Sci.*, 2022, **208**, 110614.

32 D. Wang, C. Yang, B. Zheng, M. Yang, Y. Guo, Y. Jin, Y. Dong, P. Liu, M. Zhang, E. Zhou, T. Gu, D. Xu and F. Wang, Microbiologically influenced corrosion of CoCrFeMnNi high entropy alloy by sulfate-reducing bacterium *Desulfovibrio vulgaris*, *Corros. Sci.*, 2023, **223**, 111429.

33 M. Arroussi, K. Yang, A. Shams, I. U. H. Toor and B. Wei, Advances in microbial corrosion of metals induced via extracellular electron transfer by Shewanella oneidensis MR-1, *npj Mater. Degrad.*, 2025, **9**, 47.

34 H. Bai, Y. Kang, H. Quan, Y. Han, J. Sun and Y. Feng, Treatment of acid mine drainage by sulfate reducing bacteria with iron in bench scale runs, *Bioresour. Technol.*, 2013, **128**, 818–822.

35 Z. Li, J. Yang, S. Lu, W. Dou and T. Gu, Mitigation of Desulfovibrio ferrophilus IS5 degradation of X80 carbon steel mechanical properties using a green biocide, *Biodegradation*, 2024, **35**, 439–449.

36 L. Fan, Y. Sun, D. Wang, Y. Zhang, M. Zhang, E. Zhou, D. Xu and F. Wang, Microbiologically influenced corrosion of a novel pipeline steel containing Cu and Cr elements in the presence of *Desulfovibrio vulgaris* Hildenborough, *Corros. Sci.*, 2023, **223**, 111421.

37 O. O. Ekerenam, A. L. Ma, Y. G. Zheng, S. Y. He and P. C. Okafor, Evolution of the corrosion product film and its effect on the erosion-corrosion behavior of two commercial 90Cu-10Ni tubes in seawater, *Acta Metall. Sin.*, 2018, **31**, 1148–1170.

38 M. Fu, X. Cheng, J. Li, S. Chen, W. Dou and G. Liu, Influence of soluble, loosely bound and tightly bound extracellular polymeric substances (EPS) produced by *Desulfovibrio vulgaris* on EH40 steel corrosion, *Corros. Sci.*, 2023, **221**, 111342.

39 X. Liu, Y. Wang, Y. Song, W. Liu, J. Zhang, N. Li, K. Dong, Y. Cai and E. H. Han, The respective roles of sulfate-reducing bacteria (SRB) and iron-oxidizing bacteria (IOB) in the mixed microbial corrosion process of carbon steel pipelines, *Corros. Sci.*, 2024, **240**, 112479.